

Article

A Neutral Pyridine-Pyrazole-Based N^{*}N^{*}N^{*}N Ligand as a Tetradentate Chromophore for Diverse Transition Metal Cations

Tobias Theiss ^{1,2}, María Victoria Cappellari ^{1,2}, Jutta Kösters ¹, Alexander Hepp ^{1,2} and Cristian A. Strassert ^{1,2,*}

¹ Institut für Anorganische und Analytische Chemie, Universität Münster, Corrensstraße 28/30, 48149 Münster, Germany

² CiMIC, SoN, CeNTech, Universität Münster, Heisenbergstraße 11, 48149 Münster, Germany

* Correspondence: ca.s@uni-muenster.de

Abstract: Herein, the synthesis and the structural as well as the photophysical characterization of five transition metal complexes bearing a neutral pyridine-pyrazole-based N^{*}N^{*}N^{*}N ligand (L) acting as a tetradentate chelator are reported. The luminophore can be synthesized via two different pathways. An alkyl chain with a terminal *tert*-butyl moiety was inserted on the bridging nitrogen atom to enhance the solubility of the complexes in organic solvents. Due to the neutral character of L, metal ions with different charges and electronic configurations can be chelated. Thus, complexes with Pt(II) (C1), Ag(I) (C2), Zn(II) (C3), Co(II) (C4) and Fe(II) (C5) were synthesized. Single-crystal X-ray diffraction experiments showed that complex C2 exhibits a completely different structure in the crystalline state if compared with C3 and C5, i.e., depending on the chelated cation. The UV-vis absorption and the NMR spectra showed that the complexes dissociate in liquid solutions, except for the Pt(II)-based coordination compound. Therefore, the photophysical properties of the complexes and of the ligand were studied in the solid state. For the Pt(II)-based species, a characteristic metal-perturbed ligand-centered phosphorescence was traceable, both in dilute solutions as well as in the solid state.

Keywords: pyridine-pyrazole-based N^{*}N^{*}N^{*}N ligand; transition metal complexes; time-resolved and steady-state photoluminescence spectroscopy; synthesis; structural characterization



Citation: Theiss, T.; Cappellari, M.V.; Kösters, J.; Hepp, A.; Strassert, C.A. A Neutral Pyridine-Pyrazole-Based N^{*}N^{*}N^{*}N Ligand as a Tetradentate Chromophore for Diverse Transition Metal Cations. *Inorganics* **2024**, *12*, 27. <https://doi.org/10.3390/inorganics12010027>

Academic Editors: Wolfgang Linert, Gabriel García Sánchez, David Turner and Koichiro Takao

Received: 31 October 2023

Revised: 5 December 2023

Accepted: 18 December 2023

Published: 10 January 2024



Copyright: © 2024 by the authors. Licensee MDPI, Basel, Switzerland. This article is an open access article distributed under the terms and conditions of the Creative Commons Attribution (CC BY) license (<https://creativecommons.org/licenses/by/4.0/>).

1. Introduction

Mono- and bis-cyclometalated transition metal complexes have been extensively studied in the past few decades. In particular, compounds with heavy transition metals, such as Pt(II) [1,2], Ir(III) [3,4] and Os(II) [5,6], are widely used in optoelectronics [7–9], bioimaging [10,11] and in anticancer therapy [12–14] due to their outstanding physical and chemical properties. However, lighter metal ions, such as Zn²⁺, Cu²⁺ and Fe²⁺, cannot be complexed via cyclometalation, or only under difficult conditions. Therefore, other options to synthesize the corresponding complexes have been investigated as well. Porphyrins provide a well-studied class of coordination environments. These compounds consist of four pyrrole rings that are cyclically connected via methine bridges [15,16]. A non-cyclometalating NNNN dianionic chromophore is optimal for the complexation of di-cations like Fe²⁺ or Mg²⁺. Tetrapyrrolates have a high biological relevance, as several proteins bear a porphyrin-based prosthetic group and coordinate different metal cations, depending on their function. For example, the hemoglobin required for oxygen transport has an Fe²⁺ metal center, whereas the chlorophyll in photosystems contains a Mg²⁺ center [17–20]. Another class of ligands that provide non-cyclometalating NNNN coordination environments are represented by phthalocyaninates (Pcs). These are synthesized by the cyclotetramerization of phthalic acid and its derivatives. Many phthalocyanine-based complexes (MPcs) can be used in different ways, including catalysis [21,22] and photodynamic therapy [23,24], among others.

Inspired by the chemical structures of porphyrines and phthalocyanines, we focused on the synthesis of a neutral N⁴ chromophore. Dianionic N⁴ ligands based on a 2-(1*H*-pyrazol-5-yl)pyridine unit have been developed in the past (see Figure 1A). As they do not yield a macrocyclic coordination environment, Os(II) [25] and Pt(II) [26,27] were successfully chelated under relatively mild conditions. Since we wanted to develop a ligand able to support metal ions with a wide variety of electronic configurations and charges, we herein decided to focus on a neutral N⁴ chelator. In comparison to the complexes already published, this concept exhibits a 2-(1*H*-pyrazol-1-yl)pyridine motif. In this regard, an inspiring example has been already described by Xie et al. (see Figure 1B) [28], where 4,4'-dipyridyl-amine (4,4'-dpa) was used as a key part of the bridging unit. The nitrogen atoms of this moiety constitute additional binding sites for the formation of coordination polymers. Thereby, 3D assemblies with Zn(II), Cd(II), Co(II) and Cu(II) centers and different anions were obtained.

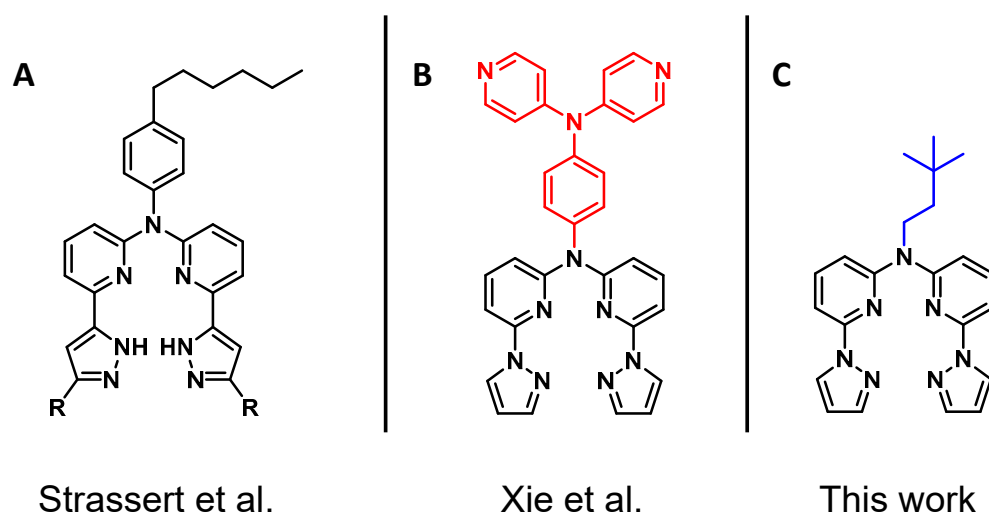


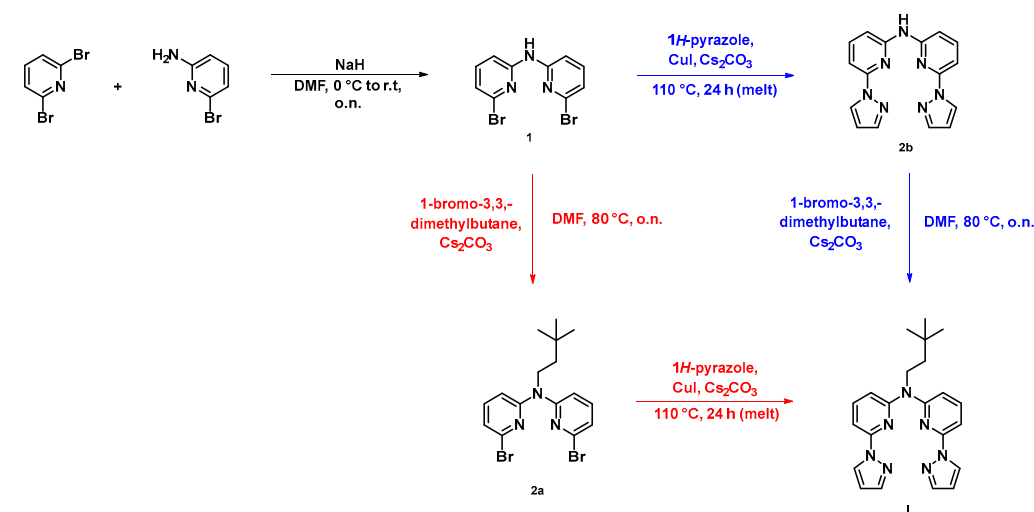
Figure 1. (A) Dianionic ligand precursor based on a pyridine-pyrazole published by Strassert et al. [26]. (B) Ligand reported by Xie et al. with a 4,4'-dpa bridging unit (red) [28]. (C) The herein presented ligand contains an alkyl chain with a *tert*-butyl group (blue).

In this report, we present the synthesis as well as the structural and photophysical characterization of five transition metal complexes based on a pyridine-pyrazole-based N⁴ ligand. For the decoration of the chelator, we chose an alkyl chain with a terminal *tert*-butyl group on the bridging position instead of a 4,4'-dpa unit (see Figure 1C). This moiety prevents the formation of coordination polymers. Moreover, it increases the solubility and crystallinity of the complexes. Based on this ligand, five transition metal complexes were synthesized with different electronic configurations. Among the 3*d*-block elements, Fe²⁺ (*d*⁶), Co²⁺ (*d*⁷) and Zn²⁺ (*d*¹⁰) were used, while the 4*d*-ion Ag⁺ (*d*¹⁰) and the 5*d*-row species Pt²⁺ (*d*⁸) were explored as well. The five transition metal complexes as well as all four organic precursors were fully characterized by nuclear magnetic resonance (NMR) spectroscopy and mass spectrometry (EM-MS). To investigate the structural properties, crystalline samples of one precursor and three coordination compounds (Ag(I), Zn(II) and Fe(II) complexes) were analyzed by single-crystal X-ray diffraction (XRD) experiments. Moreover, the photophysical characterization was carried out at room temperature in the solid state. In the case of the kinetically stable Pt(II) complex **C1**, the photoluminescence was also explored in liquid solutions at room temperature as well as in frozen glassy matrices at 77 K.

2. Results and Discussion

2.1. Synthesis

The synthesis of the N[∗]N[∗]N[∗]N ligand (**L**), as well as of the intermediates **1**, **2a** and **2b**, is shown in Scheme 1. Starting from commercially available 2,6-dibromopyridine and 2-amino-6-bromopyridine, bis(6-bromopyridine-2-yl)amine (**1**) was synthesized by optimizing previously reported procedures [29–31]. To a cooled DMF solution of 2-amino-6-bromopyridine, sodium hydride was added as a deprotonating agent (caution: flammable H₂ formation with gas evolution). After adding the second pyridine derivate, the solution was allowed to reach room temperature overnight. After quenching the remaining hydride with water (caution: flammable H₂ formation with gas evolution), the precipitated solid was filtered off and washed with cold water. After purification via column chromatographic separation, **1** was obtained with yields reaching 54%. The synthesis of **1** was carried out on a multigram scale. To realize **L** proceeding from **1**, two different synthetic pathways are possible. The first option is the alkylation of **1** using 1-bromo-3,3-dimethylbutane to yield **2a**, followed by an Ullman-like CuI-catalyzed reaction with pyrazole to obtain **L**. For the synthesis of **2a**, Cs₂CO₃ was used to deprotonate **1**; the corresponding alkylation reagent was 1-bromo-3,3-dimethylbutane to install the advantageous bridging unit (with enhanced solubility and crystallinity). After removing the remaining carbonate and the solvent, **2a** was obtained after column chromatographic separation with excellent yields (91%). In the following step, the pyrazole moiety was connected in a Cu(I)-catalyzed reaction. In this solvent-free reaction, the ligand **L** was obtained with yields reaching 70%. The alkylation, as well as the Ullmann-like reaction, was carried out as reported previously [28,30].

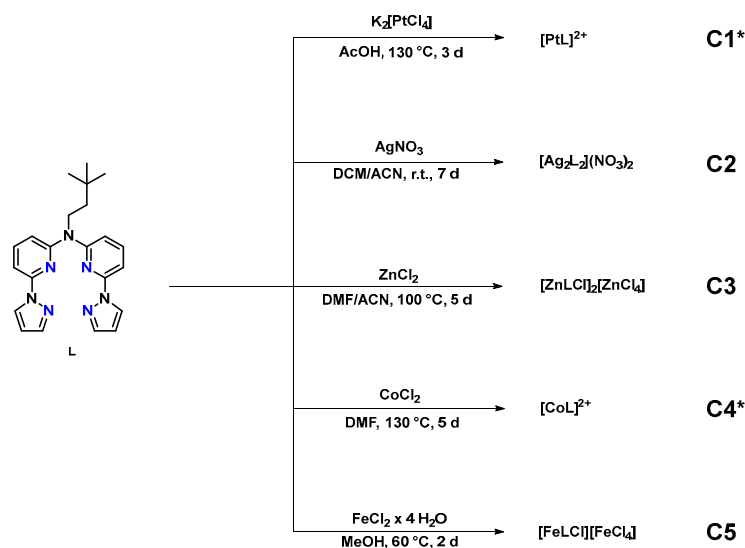


Scheme 1. Synthesis of **L** via two different routes.

The second option is to switch these two steps: After installing the pyrazole moiety (**2b**, 48%), the alkylation of the secondary amine is the final step to realize the N[∗]N[∗]N[∗]N ligand (**L**, 83%). Regarding the overall yield, the reaction pathway via **2a** is more effective. Moreover, the purification via column chromatography of the secondary amine (**2b**) is less straightforward if compared with the tertiary amine (**2a**).

The synthesis of the five transition metal complexes **C1–C5** starting from **L** is shown in Scheme 2. The complexes were obtained by adapting and optimizing previously reported procedures [28]. For the dications (in **C1** and **C3–C5**), the corresponding chlorides were used as metal precursors. Several experiments with the rather insoluble Ag(I) chloride to obtain **C2** were not successful; thus, other Ag⁺ sources were tested. With Ag(I) nitrate, **C2** was formed. It should be noted that a light-protected environment (during the synthesis and for follow-up experiments) is mandatory when using Ag(I)-based compounds. While the reaction conditions towards **C2–C5** are rather mild, those required to obtain **C1** are harsher, as reported for other platination reactions. Interestingly, the bis-cyclometalated

Pt(II) complex was not observed, meaning that the coordination of the N-atoms prevails over CH-activation. The purification of the products was not possible by column chromatography due to the charged character of the complexes. Therefore, all the complexes were crystallized and washed with suitable solvents, as **L** showed a significantly higher solubility in organic solvents than the complexation products **C1–C5**.



Scheme 2. Synthesis of the Pt(II), Ag(I), Zn(II), Co(II) and Fe(II) complexes starting from **L**. * Since the molecular structure in a single crystal could not be determined for **C1** and **C4**, an exact specification of the composition of the complexes is not possible; thus, chloride counter-anions are plausibly expected.

All compounds (**1**, **2a**, **2b**, **L** and **C1–C5**) were characterized by nuclear magnetic resonance (NMR) spectroscopy (1D and 2D experiments) as well as by exact mass spectrometry (EM-MS). The corresponding spectra can be found in the Supplementary Materials (Figures S1–S73). For **1**, **L**, **C2**, **C3** and **C5**, single crystals suitable for X-ray diffraction measurements were obtained by slow evaporation of the solvent from saturated solutions. Detailed experimental procedures and additional structural information can be found in the Supplementary Materials.

2.2. Structural Characterization

All compounds were characterized by NMR spectroscopy, where all signals were unambiguously assigned based on the results from 2D-NMR experiments. Due to the N[∞]N[∞]N[∞] coordination pattern, there are only minor differences between the ¹H-NMR spectra of the ligand (**L**) and the complexes **C1–C5**; nonetheless, some general aspects can be extracted. The ¹H-NMR spectra of **L** and **C1–C5** show the same peaks, with identical intensities and chemical shifts. The most prominent signal is the sharp singlet with an intensity of about *I* = 9 in the aliphatic range, which is due to the *tert*-butyl group. The two additional signals below δ = 5.0 ppm with a multiplet structure can be assigned to the aliphatic chain (positions H₈ and H₉). The chemical shifts of the aromatic protons resulting from the pyridine and pyrazole units were detected in a range between 6.5 ppm and 9.5 ppm. For the Pt(II) complex **C1**, the corresponding signal was observed in the ¹⁹⁵Pt-NMR spectrum (δ = −2867 ppm). The ¹H-NMR spectra of **C4** and **C5** show broad signals; thus, no coupling constants (*J*) can be determined. The broad signals are consistent with the presence of a paramagnetic species. Since the results of the NMR spectra themselves cannot give an unambiguous proof of the structures, additional experiments were carried out.

The synthetic precursor **1**, the ligand **L**, the Ag(I) complex (**C2**), the Zn(II) derivative (**C3**) and the Fe(II) compound (**C5**) were structurally characterized by single-crystal XRD analysis (see Figures 2–4). More detailed information related to the XRD data can be found in the Supplementary Materials (see Tables S1–S4 and Figures S74–S87).

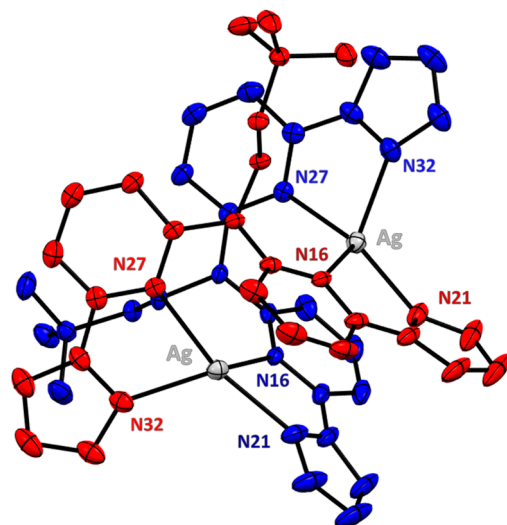


Figure 2. Molecular structure in a single crystal of C2 (located on a crystallographic two-fold axis). Hydrogen atoms, counter-ions ($2 \times \text{NO}_3^-$) and solvent molecules have been omitted for clarity. For better illustration, the two ligands were colored in red and blue, whereas the Ag^+ cations are presented in grey. Displacement ellipsoids are shown at 50% probability.

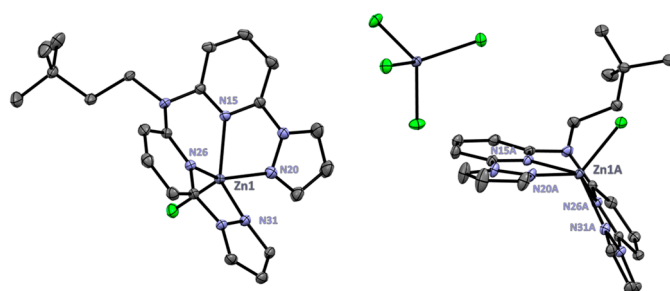


Figure 3. Asymmetric unit of C3. Hydrogen atoms and solvent molecules have been omitted for clarity. Displacement ellipsoids are shown at 50% probability. Chlorine atoms are depicted in green.

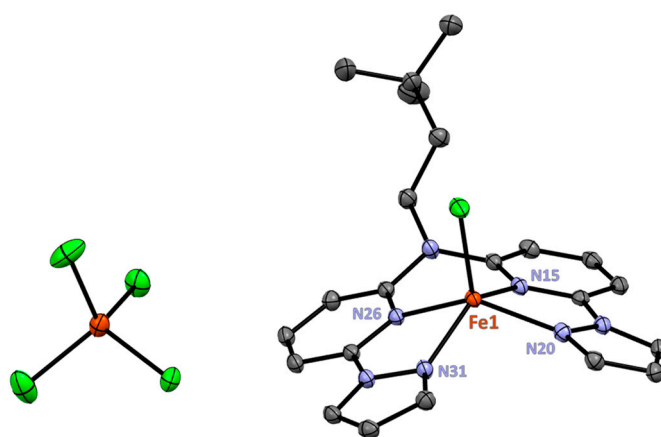


Figure 4. Molecular structure in the single crystal of C5. Hydrogen atoms and solvent molecules have been omitted for clarity. Displacement ellipsoids are shown at 50% probability. Chlorine atoms are depicted in green.

Even though it was initially expected that the respective metal ion would be chelated in the center of the N^{*}N^{*}N^{*}N ligand by the pyridine-pyrazole moieties and accompanied by one (for **C2**) or two counter-anions (for **C1** and **C3–C5**), the investigated complexes displayed characteristic structural features in their crystalline phases. Notably, the Ag(I) complex **C2** (see Figure 2) represents a dinuclear species located around a two-fold crystallographic axis. Each Ag(I) cation is tetracoordinated by two pyridine-pyrazole motifs from two different ligands, leading to a twisted structure. Besides the Ag(I) complexes, two disordered nitrate anions and a water molecule are included in the structure. The Ag-N bond distances are similar for both Ag(I) centers and in a range between 2.240 Å and 2.426 Å. In order to better illustrate this fact, the two ligand species are presented in different colors (red and blue) in Figure 2.

The X-ray diffraction study on the Zn(II) complex **C3** (see Figure 3) showed the asymmetric unit comprising two similar entities with an axially bound chlorido ligand each (charge-counterbalanced by a tetrachloridozincate(II) species ([ZnCl₄]²⁻), as well as a lattice methanol molecule. Although both Zn(II) complexes in the asymmetric unit show similar geometries, they differ in some structural details. One molecule shows Zn1-N bonds in a range between 2.070 Å and 2.121 Å and a dihedral angle of 43.86°, based on the coordinated N^{*}N moiety. The Zn(II) center is placed slightly above the coordination plane (0.721 Å). The second complex exhibits slightly longer Zn1A-N bonds (between 2.096 Å and 2.134 Å and a dihedral angle of 53.87°), while the Zn(II) cation is displaced by 0.788 Å from the coordination plane.

The molecular structure in the single crystal of the Fe(II) complex **C5** (see Figure 4) resembles the one observed for the Zn(II) complex. The Fe(II) complex shows a distorted square-pyramidal geometry involving the N^{*}N^{*}N^{*}N donor atoms and a chlorido ligand at the axial position, while the Fe(II) ion is displaced by 0.735 Å from the basal plane (see Figure S86, Supplementary Materials). The interatomic distances within the Fe1-N bonds exhibit a variation within the range from 2.101 Å to 2.136 Å. The two coordinated N^{*}N moieties in this complex (consisting of a pyridine-pyrazole unit each) are located at a dihedral angle of 33.98° to each other (see Figure S87, Supplementary Materials). The overall charge of the complex is balanced by a tetrachloridoferrate(III) entity ([FeCl₄]¹⁻). Besides these two units, two more acetone molecules complete the asymmetric unit.

Although it was not possible to grow crystals suitable for X-ray diffractometry experiments for **C1** and **C4**, structural data can be extracted from NMR spectroscopy and mass spectrometry. For complex **C1**, the ¹⁹⁵Pt-NMR spectrum (Figure S42, Supplementary Materials) and the corresponding mass spectra (Figures S43–S44, Supplementary Materials) demonstrate the presence of a Pt(II) complex. For **C4**, the NMR spectra cannot give a definitive proof for the formation of a Co(II)-based species; however, the mass spectrum (Figure S66, Supplementary Materials) supports the assumption that a Co(II) complex is formed, as opposed to a Co(III) species.

2.3. UV-Vis Absorption and Photoluminescence Spectroscopies

In addition to UV-vis absorption, the photophysical characterization was performed by using time-resolved and steady-state photoluminescence spectroscopy. The absorption profiles in liquid solutions at room temperature (RT) as well as the luminescence spectra of the solids are shown in Figure 5, whereas luminescence spectra in liquid solutions and frozen glassy matrices are depicted in Figure 6. Time-resolved photoluminescence decays of **L** and **C1–C5** can be found in the Supplementary Materials (Figures S88–S98). Selected photophysical data are summarized in Table 1.

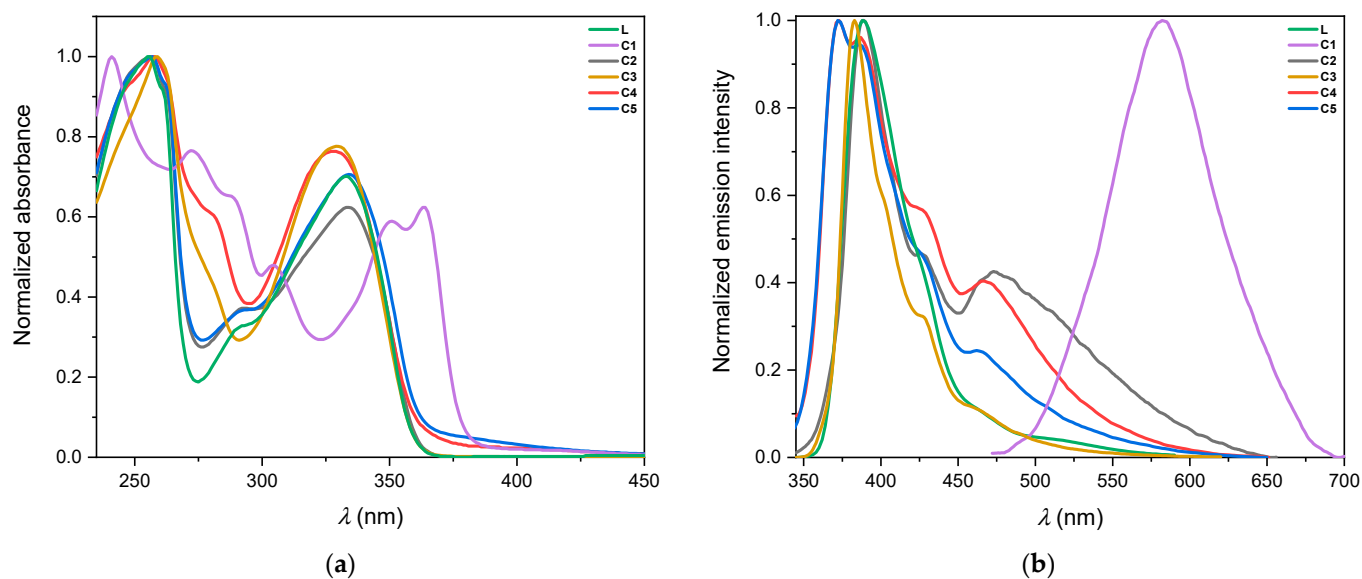


Figure 5. (a) UV-vis absorption spectra of L and C1–C5 in solution. (b) Photoluminescence spectra of L and C1–C5 at room temperature in the solid state ($\lambda_{\text{exc}} = 320\text{--}350$ nm).

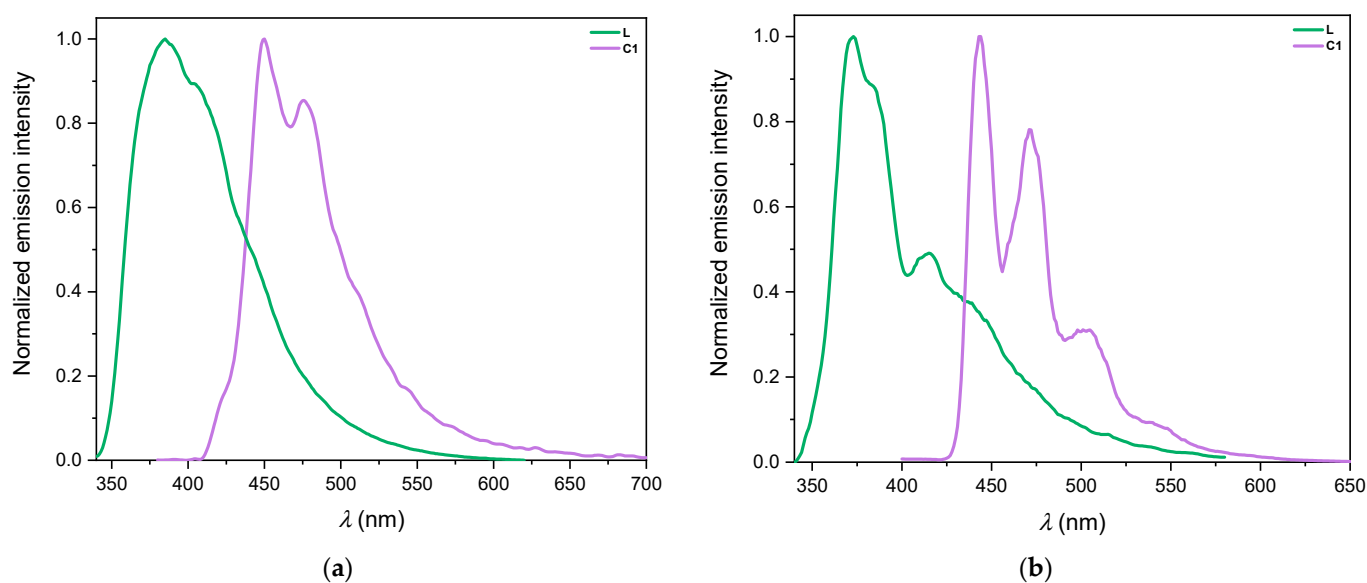


Figure 6. (a) Photoluminescence spectra of L (green) and C1 (violet) at 298 K in liquid MeOH at RT ($\lambda_{\text{exc}} = 320$ nm and $\lambda_{\text{exc}} = 350$ nm, respectively). The solution was optically diluted ($A < 0.1$). (b) Photoluminescence spectra at 77 K in a frozen glassy matrix of DCM/MeOH (V:V = 1:1, $\lambda_{\text{exc}} = 320$ nm). Spectra normalized to the highest intensity.

The UV-vis absorption spectra (Figure 5a) of L and C1–C5 in liquid solutions show bands in the range from 230 nm to 400 nm. For C2–C5, two prominent bands were detected. The strong absorption bands in the UV region (≤ 350 nm) are derived from transitions into ligand-centered ($\pi - \pi^*$) states, which are comparable to the absorption profiles presented by the free ligand, L [27]. For C1, the absorption spectrum shows a different pattern if compared with L and C2–C5. The bands at higher energies (250–275 nm) can be related to transitions into excited ligand-centered (^1LC) singlet states as well [32]. Those at lower energies (ca. 375 nm) are most likely associated with transitions into states with metal-to-ligand charge-transfer ($^1\text{MLCT}$), metal-centered (^1MC) or ligand-centered (^1LC) character [30]. The absorption spectra of solutions involving C2–C5 differ only marginally from the free ligand L. This leads to the conclusion that the complexes C2–C5

are dissociated in liquid solutions. This assumption is supported by the results from $^1\text{H-NMR}$ spectroscopy (see Supplementary Materials, Figures S45, S52, S60 and S67). In fact, the corresponding spectra—more precisely, the chemical shifts of the respective hydrogen atoms of the compounds **C2–C5**—only marginally differ from those of the free ligand **L**.

Table 1. Selected photophysical data for **L** and **C1–C5**.

Compound	298 K						77 K	
	MeOH Solution at Room Temperature			Solid State at Room Temperature			Frozen Glassy Matrix DCM/MeOH 1:1 77 K	
	λ_{em}/nm	τ/ns	Φ_L ($\pm 2\%$)	λ_{em}/nm	τ/ns	Φ_L ($\pm 2\%$)	λ_{em}/nm	τ/ns
L	384	2.75 ± 0.06	<2%	382	1.628 ± 0.007	15%	370	1.71 ± 0.02
C1	450, 480	280.2 ± 0.9 (Ar-purged); 223.9 ± 0.6 (air-eq.)	3% (Ar-purged); <2% (air-eq.)	588	$(66.0 \pm 0.3) \times 10^3$	<2%	444	285 ± 2
C2				388	8.51 ± 0.04	<2%		
C3				382	0.78 ± 0.01	<2%		
C4				372	7.5 ± 0.1	<2%		
C5				382	7.2 ± 0.1	<2%		

Due to the dissociative behavior in methanolic solutions, our investigation focused on the photoluminescence properties of both the ligand **L** and the complexes **C1–C5** in the solid state at room temperature (Figure 5b). Each complex shows different emission wavelengths and spectra, depending on the chelated cation. The ligand **L** exhibits an intense fluorescence band, with a peak at 388 nm when excited at 320 nm. This emission can be attributed to a singlet $\pi - \pi^*$ state, reaching a quantum yield of 15% [28]. The amplitude-weighted average excited-state lifetime corresponds to a fluorescent relaxation, reaching 1.628 ns.

In the case of **C1** in the solid state, it exhibited a vibronically unstructured emission spectrum with a broad peak at 588 nm, indicating the presence of metal–metal (Pt...Pt) interactions; hence, these aggregates emit from metal–metal-to-ligand charge-transfer states ($^3\text{MMLCT}$) [33]. The amplitude-weighted average lifetime of the excited state for **C1** was prominently longer, reaching 66 μs , but it is significantly shorter if compared with the average excited-state lifetime of the monomeric species in liquid solution (see Table 1). **C2** exhibited an emission spectrum with a peak at 388 nm and a shoulder at 475 nm, with a notably long average lifetime of 8.5 ns. **C3** presented an emission spectrum with a maximum at 382 nm, with a slight blue shift with respect to Ag(I) and an average lifetime of only 0.78 ns. On the other hand, **C4** and **C5** showed comparable emission spectra with a maximum at 372 nm as well as shoulders at 466 nm and 462 nm. The photoluminescence quantum yields of **C2**, **C3**, **C4** and **C5** at room temperature were below 2%.

C1 is the only kinetically stable complex in liquid solutions. For this reason, the photophysical properties were measured in a methanolic solution at room temperature as well as in a frozen glassy matrix of dichloromethane-methanol 1:1 at 77 K (Figure 6). For comparison, also the corresponding emission spectrum of **L** at both temperatures is shown. At room temperature, **C1** exhibited a well-defined emission spectrum showing the characteristic vibrational progression of Pt(II) complexes stemming from metal-perturbed ligand-centered states, with an emission maximum at 450 nm and a quantum yield of 3% (Figure 6a). The long excited-state lifetime in the microsecond range is typical for the phosphorescence of Pt(II) complexes. The presence of dissolved molecular dioxygen ($^3\text{O}_2$) shortens the values of the lifetimes and lowers the photoluminescence quantum yield (see Table 1 and Figures S94 and S95). The emission spectra at low temperature are shown in Figure 6b. The spectrum in a rigid glassy matrix at 77 K exhibited a well-defined vibrational progression and the emission lifetimes were in the microsecond range, pointing

towards triplet LC states with a perturbative MLCT character enabling the phosphorescence ($^3\text{MP-LC}$).

3. Methods and Materials

Additional information about the experimental procedures for the synthesis of **1**, **2a**, **2b**, **L** and **C1–C5**, the structural characterization (1D and 2D-NMR spectra, mass spectra and crystallographic data), as well as the time-resolved photoluminescence decays for all compounds can be found in the Supplementary Materials.

Materials: All commercially available chemicals and solvents were used as purchased. For the purification via column chromatography in the synthesis of **1**, **2a**, **2b** and **L**, silica gel 60 was used.

Synthesis: A detailed description of the synthesis (experimental procedures, reaction conditions and purification methods) can be found in the Supplementary Materials.

Structural characterization: All compounds were characterized by 1D-NMR experiments (^1H , ^{13}C , $^{13}\text{C}\{^1\text{H}\}$ DEPT135, ^{15}N and ^{195}Pt) and 2D-NMR experiments (HH-COSY, HC-HSQC and HC-HMBC). The NMR spectra were recorded at the Institut für Anorganische und Analytische Chemie (Universität Münster) using a Bruker Avance III 400, Bruker Avance Neo 400 or a Bruker Avance Neo 500. All NMR measurements were performed at 300 K. The chemical shifts (δ) of the spectra are given in parts per million (ppm). The signals are referenced to the residual proton signal in the corresponding deuterated solvents used: DCM- d_2 (^1H at 5.32 ppm/ ^{13}C at 54.00 ppm), acetone- d_6 (^1H at 2.05 ppm/ ^{13}C at 29.84 ppm), methanol- d_4 (^1H at 3.31 ppm/ ^{13}C at 49.00 ppm) and DMSO- d_6 (^1H at 2.50 ppm/ ^{13}C at 39.52 ppm). The signal multiplicities are given as s (singlet), d (doublet), t (triplet) and m (multiplet). The mass spectrometric analysis was carried out at the Institut für Anorganische und Analytische Chemie (Universität Münster) using a Bruker Impact II with electrospray ionization (ESI) to obtain exact mass (EM) spectra for all compounds (**1**, **2a**, **2b**, **L** and **C1–C5**). The samples were dissolved in MeOH and injected with an autosampler using a mixture of methanol and acetonitrile as the solvent. The corresponding NMR spectra are presented in the Supplementary Materials as well as the mass spectra for all compounds (see Figures S1–S73). The X-ray diffraction measurements were carried out at the Institut für Anorganische und Analytische Chemie (Universität Münster) using a Venture single-crystal X-ray diffractometer. The experiments were carried out at 100 K (**1**, **L**, **C2** and **C5**) or 110 K (**C3**). For **1**, **L**, **C2**, **C3** and **C5**, crystals suitable for X-ray diffraction analysis were obtained by slow evaporation of a saturated MeOH solution (**C2**, **C3**), a saturated acetone solution (**1**, **L**) and a solvent mixture of MeOH-acetone (V:V = 1:1, **C5**). The crystallization process of the Ag(I) complex **C2** was carried out in a light-protected environment. The X-ray diffractometric data reduction was carried out using SAINT+ [34]. The crystal structures were solved by using SHELXTL [35]. The molecular structures in the crystal and the unit cells were created with MERCURY [36]. A detailed summary of the crystallographic data can be found in the Supplementary Materials (Table S1 as well as Figures S74–S87). With the CCDC numbers 2286147 (**1**), 2292917 (**L**), 2286148 (**C2**), 2286153 (**C3**) and 2286154 (**C5**), supplementary crystallographic data for these structures can be accessed.

Photophysical characterization: The five transition metal complexes **C1–C5** as well as the ligand **L** were analyzed by steady-state and time-resolved photoluminescence spectroscopy. Absorption spectra were measured with a Shimadzu UV-1900i UV-VIS-NIR spectrophotometer. All solvents used were of spectrometric grade (Uvasol[®], Merck, Darmstadt, Germany). Photoluminescence quantum yields were measured with a Hamamatsu Photonics absolute PL quantum yield measurement system (C9920-02) equipped with an L9799-01 CW Xe light source (150 W), a monochromator, a C7473 photonic multi-channel analyzer and an integrating sphere and employing U6039-05 software (Hamamatsu Photonics, Ltd., Shizuoka, Japan).

Steady-state excitation and emission spectra were recorded on a FluoTime 300 spectrometer obtained from PicoQuant (Berlin, Germany) equipped with a 300 W ozone-free Xe

lamp (250–900 nm), a 10 W Xe flashlamp (250–900 nm, pulse width: ca. 1 μ s) with repetition rates of 0.1–300 Hz, a double-grating excitation monochromator (Czerny–Turner-type, grating with 1200 lines/mm, blaze wavelength: 300 nm), diode lasers (pulse width: <80 ps) operated by a computer-controlled laser driver (PDL-828 “Sepia II”; repetition rate of up to 80 MHz, burst mode for slow and weak decays), two double-grating emission monochromators (Czerny–Turner-type, selectable gratings blazed at 500 nm with 2.7 nm/mm dispersion and 1200 lines/mm, or blazed at 1200 nm with 5.4 nm/mm dispersion and 600 lines/mm) with an adjustable slit width between 25 μ m and 7 mm, as well as Glan-Thompson polarizers for excitation (after the Xe-lamps) and emission (after the sample).

For the solid state, a special sample holder for front-face (FF) measurements was used. Sample holders with a Peltier-cooled mounting unit ranging from -15 to 110 $^{\circ}$ C, along with two detectors (namely, a PMA Hybrid-07 from PicoQuant with transit time spread FWHM < 50 ps, 200–850 nm, or a H10330C-45-C3 NIR detector with transit time spread FWHM 0.4 ns, 950–1700 nm from Hamamatsu) were used. Steady-state spectra and photoluminescence lifetimes were recorded in TCSPC mode by using a PicoHarp 300 (minimum base resolution: 4 ps) or in MCS mode with a TimeHarp 260 (where up to several ms can be traced). Emission and excitation spectra were corrected for source intensity (lamp and grating) by standard correction curves. Lifetime analysis was performed using the commercial EasyTau 2 software (PicoQuant). The quality of the fit was assessed by minimizing the reduced chi-squared function (χ^2) as well as by visual inspection of the weighted residuals and their autocorrelation.

4. Conclusions

In this work, the synthesis of a pyridine-pyrazole-based $N^*N^*N^*$ ligand **L** is reported, as well as its corresponding Pt(II), Ag(I), Zn(II), Co(II) and Fe(II) complexes, namely, **C1–C5**. The complexes dissociate in solution, as observed by NMR and absorption spectroscopies. Nevertheless, the molecular structures in single crystals of **C2**, **C3** and **C5** exhibit an interesting diversity. While the dinuclear Ag(I) species **C2** shows a twisted sandwich-like structure, the Zn(II) and Fe(II) complexes (**C3** and **C5**, respectively) bind the metal ions in the central pocket of the $N^*N^*N^*$ coordination environment. Notably, the N-coordination precludes any cyclometallation via CH-activation with Pt(II).

Besides the structural characterization based on NMR spectroscopy and X-ray diffraction analysis, photophysical experiments were carried out in solution at room temperature, in frozen glassy matrices at 77 K and in the solid state. The absorption spectra in a methanolic solution of **L** and **C2–C5** show almost the same profile, most likely due to dissociation. This assumption can be confirmed via NMR spectroscopy and by the fluorescence lifetimes resembling those of **L**. Nonetheless, the Pt(II) complex **C1** showed a good stability in solution with a characteristic phosphorescence stemming from a metal-perturbed ligand-centered triplet state.

These results pave the way for novel transition metal complexes with different electronic configurations, from 3d-block to 5d-row metals. Herein, metal ions with d^6 , d^7 , d^8 and d^{10} configurations were explored; ongoing studies will provide insights regarding further configurations, such as d^1 – d^5 and d^9 .

Supplementary Materials: The following supporting information can be downloaded at <https://www.mdpi.com/article/10.3390/inorganics12010027/s1>. Section S1: Synthesis and characterization; Section S2: NMR and mass spectra; Section S3: Single-crystal X-ray diffraction data; Section S4: Photophysical characterization.

Author Contributions: Conceptualization, T.T. and C.A.S.; validation, M.V.C., T.T. and C.A.S.; formal analysis, T.T. and M.V.C.; NMR-measurements, A.H.; NMR-structure analysis, A.H. and T.T.; X-ray diffractometry and structure solution, J.K.; photophysical investigation, M.V.C.; resources, C.A.S.; data curation, T.T. and M.V.C.; writing—original draft preparation, T.T. and M.V.C.; writing—review and editing, T.T., M.V.C. and C.A.S.; visualization, T.T. and M.V.C.; supervision, C.A.S.; project administration, C.A.S.; funding acquisition, C.A.S. All authors have read and agreed to the published version of the manuscript.

Funding: C.A.S. gratefully acknowledges funding from the Deutsche Forschungsgemeinschaft (DFG, German Research Foundation)—Project ID 433682494—SFB 1459 “Intelligent Matter”, as well as Project STR 1186/6-2 within the Priority Programme 2102 “Light-controlled reactivity of metal complexes”. C.A.S. gratefully acknowledges the generous financial support for the acquisition of an “Integrated Confocal Luminescence Spectrometer with Spatiotemporal Resolution and Multiphoton Excitation” (DFG/Land NRW: INST 211/915-1 FUGG; DFG EXC1003: “Berufungsmittel”).

Data Availability Statement: CCDC numbers 2286147 (1), 2292917 (L), 2286148 (C2), 2286153 (C3) and 2286154 (C5) contain the supplementary crystallographic data for this paper. These data can be obtained free of charge via <http://www.ccdc.cam.ac.uk/conts/retrieving.html> (or from the CCDC, 12 Union Road, Cambridge CB2 1EZ, UK; fax: +44 1223 336033; e-mail: deposit@ccdc.cam.ac.uk).

Conflicts of Interest: The authors declare no conflicts of interest.

References

1. Theiss, T.; Buss, S.; Maisuls, I.; López-Arteaga, R.; Brünink, D.; Kösters, J.; Hepp, A.; Doltsinis, N.L.; Weiss, E.A.; Strassert, C.A. Room-Temperature Phosphorescence from Pd(II) and Pt(II) Complexes as Supramolecular Luminophores: The Role of Self-Assembly, Metal-Metal Interactions, Spin-Orbit Coupling, and Ligand-Field Splitting. *J. Am. Chem. Soc.* **2023**, *145*, 3937–3951. [[CrossRef](#)] [[PubMed](#)]
2. Tam, A.Y.-Y.; Tsang, D.P.-K.; Chan, M.-Y.; Zhu, N.; Yam, V.W.-W. A luminescent cyclometalated platinum(II) complex and its green organic light emitting device with high device performance. *Chem. Commun.* **2011**, *47*, 3383–3385. [[CrossRef](#)] [[PubMed](#)]
3. Shi, H.; Wang, Y.; Lin, S.; Lou, J.; Zhang, Q. Recent development and application of cyclometalated iridium(III) complexes as chemical and biological probes. *Dalton Trans.* **2021**, *50*, 6410–6417. [[CrossRef](#)] [[PubMed](#)]
4. Yuan, H.; Han, Z.; Chen, Y.; Qi, F.; Fang, H.; Guo, Z.; Zhang, S.; He, W. Ferroptosis Photoinduced by New Cyclometalated Iridium(III) Complexes and Its Synergism with Apoptosis in Tumor Cell Inhibition. *Angew. Chem.* **2021**, *133*, 8255–8262. [[CrossRef](#)]
5. Chi, Y.; Chou, P.-T. Contemporary progresses on neutral, highly emissive Os(II) and Ru(II) complexes. *Chem. Soc. Rev.* **2007**, *36*, 1421–1431. [[CrossRef](#)]
6. Hernández-García, A.; Marková, L.; Santana, M.D.; Prachařová, J.; Bautista, D.; Kostrhunová, H.; Novohradský, V.; Brabec, V.; Ruiz, J.; Kašpárková, J. Cyclometalated Benzimidazole Osmium(II) Complexes with Antiproliferative Activity in Cancer Cells Disrupt Calcium Homeostasis. *Inorg. Chem.* **2023**, *62*, 6474–6487. [[CrossRef](#)]
7. Au, V.K.-M.; Wong, K.M.-C.; Tsang, D.P.-K.; Chan, M.-Y.; Zhu, N.; Yam, V.W.-W. High-Efficiency Green Organic Light-Emitting Devices Utilizing Phosphorescent Bis-Cyclometalated Alkynylgold(III) Complexes. *J. Am. Chem. Soc.* **2010**, *132*, 14273–14278. [[CrossRef](#)]
8. Fleetham, T.; Li, G.; Li, J. Phosphorescent Pt(II) and Pd(II) Complexes for Efficient, High-Color-Quality, and Stable OLEDs. *Adv. Mater.* **2017**, *29*, 1601861. [[CrossRef](#)]
9. Tseng, C.-H.; Fox, M.A.; Liao, J.-L.; Ku, C.-H.; Sie, Z.-T.; Chang, C.-H.; Wang, J.-Y.; Chen, Z.-N.; Lee, G.-H.; Chi, Y. Luminescent Pt(II) complexes featuring imidazolylidene-pyridylidene and dianionic bipyrazolate: From fundamentals to OLED fabrications. *J. Mater. Chem. C* **2017**, *5*, 1420–1435. [[CrossRef](#)]
10. Septiadi, D.; Aliprandi, A.; Mauro, M.; de Cola, L. Bio-imaging with neutral luminescent Pt(II) complexes showing metal...metal interactions. *RSC Adv.* **2014**, *4*, 25709–25718. [[CrossRef](#)]
11. Jin, C.; Liang, F.; Wang, J.; Wang, L.; Liu, J.; Liao, X.; Rees, T.W.; Yuan, B.; Wang, H.; Shen, Y.; et al. Rational Design of Cyclometalated Iridium(III) Complexes for Three-Photon Phosphorescence Bioimaging. *Angew. Chem.* **2020**, *132*, 16121–16125. [[CrossRef](#)]
12. Han, X.; Sun, J.; Wang, Y.; He, Z. Recent Advances in Platinum (IV) Complex-Based Delivery Systems to Improve Platinum (II) Anticancer Therapy. *Med. Res. Rev.* **2015**, *35*, 1268–1299. [[CrossRef](#)] [[PubMed](#)]
13. Hussain, Y.; Islam, L.; Khan, H.; Filosa, R.; Aschner, M.; Javed, S. Curcumin-cisplatin chemotherapy: A novel strategy in promoting chemotherapy efficacy and reducing side effects. *Phytother. Res.* **2021**, *35*, 6514–6529. [[CrossRef](#)] [[PubMed](#)]
14. Kuang, S.; Liao, X.; Zhang, X.; Rees, T.W.; Guan, R.; Xiong, K.; Chen, Y.; Ji, L.; Chao, H. Ferrilridium: A Lysosome-Targeting Iron(III)-Activated Iridium(III) Prodrug for Chemotherapy in Gastric Cancer Cells. *Angew. Chem.* **2020**, *132*, 3341–3347. [[CrossRef](#)]
15. Misra, R.; Chandrashekar, T.K. Structural diversity in expanded porphyrins. *Acc. Chem. Res.* **2008**, *41*, 265–279. [[CrossRef](#)] [[PubMed](#)]
16. Sekaran, B.; Misra, R. β -Pyrrole functionalized porphyrins: Synthesis, electronic properties, and applications in sensing and DSSC. *Coord. Chem. Rev.* **2022**, *453*, 214312. [[CrossRef](#)]
17. Antonini, E.; Brunori, M. Hemoglobin. *Annu. Rev. Biochem.* **1970**, *39*, 977–1042. [[CrossRef](#)]
18. Ahmed, M.H.; Ghatge, M.S.; Safo, M.K. Hemoglobin: Structure, Function and Allostery. *Subcell. Biochem.* **2020**, *94*, 345–382.
19. Humphrey, A.M. Chlorophyll. *Food Chem.* **1980**, *5*, 57–67. [[CrossRef](#)]
20. Hörtensteiner, S. Update on the biochemistry of chlorophyll breakdown. *Plant Mol. Biol.* **2013**, *82*, 505–517. [[CrossRef](#)]
21. Wang, X.; Cai, Z.-F.; Wang, Y.-Q.; Feng, Y.-C.; Yan, H.-J.; Wang, D.; Wan, L.-J. In Situ Scanning Tunneling Microscopy of Cobalt-Phthalocyanine-Catalyzed CO₂ Reduction Reaction. *Angew. Chem. Int. Ed.* **2020**, *59*, 16098–16103. [[CrossRef](#)] [[PubMed](#)]

22. Lin, L.; Li, H.; Yan, C.; Li, H.; Si, R.; Li, M.; Xiao, J.; Wang, G.; Bao, X. Synergistic Catalysis over Iron-Nitrogen Sites Anchored with Cobalt Phthalocyanine for Efficient CO₂ Electroreduction. *Adv. Mater.* **2019**, *31*, 1903470. [[CrossRef](#)] [[PubMed](#)]
23. Lo, P.-C.; Rodríguez-Morgade, M.S.; Pandey, R.K.; Ng, D.K.P.; Torres, T.; Dumoulin, F. The unique features and promises of phthalocyanines as advanced photosensitisers for photodynamic therapy of cancer. *Chem. Soc. Rev.* **2020**, *49*, 1041–1056. [[CrossRef](#)] [[PubMed](#)]
24. Oshiro-Junior, J.A.; Sato, M.R.; Boni, F.I.; Santos, K.L.M.; de Oliveira, K.T.; de Freitas, L.M.; Fontana, C.R.; Nicholas, D.; McHale, A.; Callan, J.F.; et al. Phthalocyanine-loaded nanostructured lipid carriers functionalized with folic acid for photodynamic therapy. *Mater. Sci. Eng. C* **2020**, *108*, 110462. [[CrossRef](#)] [[PubMed](#)]
25. Chang, S.-H.; Chang, C.-F.; Liao, J.-L.; Chi, Y.; Zhou, D.-Y.; Liao, L.-S.; Jiang, T.-Y.; Chou, T.-P.; Li, E.Y.; Lee, G.-H.; et al. Emissive osmium(II) complexes with tetradentate bis(pyridylpyrazolate) chelates. *Inorg. Chem.* **2013**, *52*, 5867–5875. [[CrossRef](#)] [[PubMed](#)]
26. Cnudde, M.; Brünink, D.; Doltsinis, N.L.; Strassert, C.A. Tetradentate N⁺N⁺N⁺N⁺-type luminophores for Pt(II) complexes: Synthesis, photophysical and quantum-chemical investigation. *Inorg. Chim. Acta* **2021**, *518*, 120090. [[CrossRef](#)]
27. Liao, K.-Y.; Hsu, C.-W.; Chi, Y.; Hsu, M.-K.; Wu, S.-W.; Chang, C.-H.; Liu, S.-H.; Lee, G.-H.; Chou, P.-T.; Hu, Y.; et al. Pt(II) metal complexes tailored with a newly designed spiro-arranged tetradentate ligand; harnessing of charge-transfer phosphorescence and fabrication of sky blue and white OLEDs. *Inorg. Chem.* **2015**, *54*, 4029–4038. [[CrossRef](#)]
28. Ding, C.; Rui, X.; Wang, C.; Xie, Y. Coordination polymers of a multipyridyl and pyrazolyl ligand with conformational flexibility: Syntheses, structures and luminescence. *CrystEngComm* **2014**, *16*, 1010–1019. [[CrossRef](#)]
29. van der Ende, M.; Wang, D.; Frey, W.; Buchmeiser, M.R. Pentamethylcyclopentadienyl Titanium(IV) Amido Pyridylene Phenylene and Pentamethylcyclopentadienyl Titanacyclopropane Amido Complexes and their Behavior in the Polymerization of Ethylene and Cyclic Olefins. *ChemCatChem* **2017**, *9*, 1242–1252. [[CrossRef](#)]
30. Buss, S.; Cappellari, M.V.; Hepp, A.; Kösters, J.; Strassert, C.A. Modification of the Bridging Unit in Luminescent Pt(II) Complexes Bearing C⁺N⁺N⁺ and C⁺N⁺N⁺C Ligands. *Chemistry* **2023**, *5*, 1243–1255. [[CrossRef](#)]
31. Zhang, E.-X.; Wang, D.-X.; Huang, Z.-T.; Wang, M.-X. Synthesis of (NH)(m)(NMe)(4-m)-bridged calix4pyridines and the effect of NH bridge on structure and properties. *J. Org. Chem.* **2009**, *74*, 8595–8603. [[CrossRef](#)] [[PubMed](#)]
32. Hebenbrock, M.; González-Abradelo, D.; Hepp, A.; Meadowcroft, J.; Lefringhausen, N.; Strassert, C.A.; Müller, J. Influence of the ancillary ligands on the luminescence of platinum(II) complexes with a triazole-based tridentate C⁺N⁺N⁺ luminophore. *Inorg. Chim. Acta* **2021**, *516*, 119988. [[CrossRef](#)]
33. Strassert, C.A.; Mauro, M.; de Cola, L. Photophysics of soft and hard molecular assemblies based on luminescent complexes. *Adv. Inorg. Chem.* **2011**, *63*, 47–103.
34. Saint (Version 8.40B), Area Detector Control and Integration Software. Bruker AXS Inc.: Madison, WI, USA, 2021.
35. Sheldrick, G.M. A short history of SHELX. *Acta Crystallogr.* **2008**, *A64*, 112–122. [[CrossRef](#)]
36. Bruno, I.J.; Cole, J.C.; Edgington, P.R.; Kessler, M.; Macrae, C.F.; McCabe, P.; Pearson, J.; Taylor, R. New software for searching the Cambridge Structural Database and visualizing crystal structures. *Acta Crystallogr.* **2002**, *B58*, 389–397. [[CrossRef](#)]

Disclaimer/Publisher’s Note: The statements, opinions and data contained in all publications are solely those of the individual author(s) and contributor(s) and not of MDPI and/or the editor(s). MDPI and/or the editor(s) disclaim responsibility for any injury to people or property resulting from any ideas, methods, instructions or products referred to in the content.